EUROPEAN SOCIETY OF RADIOLOGY
European Radiology

GASTROINTESTINAL

Automated graded prognostic assessment for patients with hepatocellular carcinoma using machine learning

Moritz Gross[1,2*], Stefan P. Haider[1,3], Tal Ze'evi[1,4], Steffen Huber[1], Sandeep Arora[1], Ahmet S. Kucukkaya[1,2], Simon Iseke[1,5], Bernhard Gebauer[2], Florian Fleckenstein[2], Marc Dewey[2], Ariel Jaffe[6], Mario Strazzabosco[6], Julius Chapiro[1] and John A. Onofrey[1,4,7]

Abstract

Background Accurate mortality risk quantification is crucial for the management of hepatocellular carcinoma (HCC); however, most scoring systems are subjective.

Purpose To develop and independently validate a machine learning mortality risk quantification method for HCC patients using standard-of-care clinical data and liver radiomics on baseline magnetic resonance imaging (MRI).

Methods This retrospective study included all patients with multiphasic contrast-enhanced MRI at the time of diagnosis treated at our institution. Patients were censored at their last date of follow-up, end-of-observation, or liver transplantation date. The data were randomly sampled into independent cohorts, with 85% for development and 15% for independent validation. An automated liver segmentation framework was adopted for radiomic feature extraction. A random survival forest combined clinical and radiomic variables to predict overall survival (OS), and performance was evaluated using Harrell's C-index.

Results A total of 555 treatment-naïve HCC patients (mean age, 63.8 years ± 8.9 [standard deviation]; 118 females) with MRI at the time of diagnosis were included, of which 287 (51.7%) died after a median time of 14.40 (interquartile range, 22.23) months, and had median followed up of 32.47 (interquartile range, 61.5) months. The developed risk prediction framework required 1.11 min on average and yielded C-indices of 0.8503 and 0.8234 in the development and independent validation cohorts, respectively, outperforming conventional clinical staging systems. Predicted risk scores were significantly associated with OS ($p < .00001$ in both cohorts).

Conclusions Machine learning reliably, rapidly, and reproducibly predicts mortality risk in patients with hepatocellular carcinoma from data routinely acquired in clinical practice.

Clinical relevance statement Precision mortality risk prediction using routinely available standard-of-care clinical data and automated MRI radiomic features could enable personalized follow-up strategies, guide management decisions, and improve clinical workflow efficiency in tumor boards.

Key Points

- *Machine learning enables hepatocellular carcinoma mortality risk prediction using standard-of-care clinical data and automated radiomic features from multiphasic contrast-enhanced MRI.*

*Correspondence:
Moritz Gross
moritz.gross@charite.de
Full list of author information is available at the end of the article

Springer

• *Automated mortality risk prediction achieved state-of-the-art performances for mortality risk quantification and outperformed conventional clinical staging systems.*

• *Patients were stratified into low, intermediate, and high-risk groups with significantly different survival times, generalizable to an independent evaluation cohort.*

Keywords Hepatocellular carcinoma, Risk assessment, Magnetic resonance imaging, Medical image processing, Machine learning

Introduction

Liver cancer is the second most frequent cause of cancer-related death in the world [1] and the fifth leading cause in the United States [2]. In contrast to other cancer types, liver cancer incidence and mortality rates are rising [3, 4]. Hepatocellular carcinoma (HCC) is the most prevalent form of primary liver cancer, accounting for 70–85% of total liver cancers globally [5]. Imaging is a critical tool for diagnosing and staging of HCC. Magnetic resonance imaging (MRI) provides high spatial resolution and allows soft-tissue characterization of the liver. The liver imaging reporting and data system (LI-RADS) [6] has been developed for non-invasive diagnosis based on imaging criteria, and in most cases, HCC can be detected and diagnosed using contrast-enhanced multiphasic imaging without an invasive biopsy [7].

Various scoring and staging systems have been proposed for HCC mortality risk quantification and to stratify patients into risk categories [8–14]. However, these systems use only limited one-dimensional tumor size measurements [9–13], do not make use of quantitative imaging biomarkers, and stratify patients into different risk groups based on strict thresholds. Traditional one-dimensional tumor size measurements have major limitations in reflecting viability, actual tumor size, and growth potential [15] and are subject to rater variability. Quantitative image biomarkers, such as radiomic features, can be extracted from regions and volumes of interest from medical imaging data; however, automated segmentation methods are required for integration into clinical practice workloads. Fully automated whole liver segmentation based on deep learning has demonstrated robust, reproducible, and generalizable segmentation performance across disease stages with substantially altered liver morphology and only required processing times in the order of seconds [16].

The aim of this study was twofold: develop and validate an automated method for mortality risk quantification in HCC patients using only routinely available standard-of-care clinical variables and radiomic features derived from automated liver segmentations on baseline multiphasic contrast-enhanced MRI by means of machine learning and use this risk score to stratify patients into low, intermediate, and high-risk groups.

Materials and methods

Compliance with ethical standards

This HIPAA-compliant study was approved by the Yale School of Medicine institutional review board with full waiver of consent and conducted in accordance with the declaration of Helsinki.

Code availability

All code for the methodological implementation and the trained framework is publicly available on GitHub: https://github.com/OnofreyLab/hcc-mortality-risk

Data availability

Patient data and imaging data used in this paper cannot be shared publicly due to legal reasons.

Patient inclusion and exclusion

This retrospective study identified all patients with treatment-naïve HCC treated at our institution between the years 2008 and 2019. HCC was either proven by imaging criteria or biopsy confirmation. We included

(i) all patients >18 years old
(ii) that had multiphasic contrast-enhanced MRI at the time of diagnosis.

We excluded

(i) all patients with missing clinical information,
(ii) with no triphasic MRI acquisition or
(iii) non-diagnostic MRI.

The patients were randomly sampled into independent cohorts, with 85% for development and 15% for independent validation.

Clinical data

Clinical data were collected from the hospital's electronic health record system, and conventional clinical staging scores [8–14] were calculated. Patients were evaluated for extrahepatic metastases on chest computed tomography (CT) and bone scans at the date of diagnosis, and the following laboratory values were collected closest to the date of imaging: alpha-fetoprotein (AFP), total bilirubin, direct bilirubin, serum albumin, international normalized ratio (INR), partial thromboplastin time (PTT), sodium, and creatinine.

MRI acquisition and radiomics extraction

Multiphasic contrast-enhanced MRI was acquired using a standard institutional imaging protocol involving T1-weighted breath-hold sequences before contrast administration and 12–18 s, 60–70 s, and 3–5 min post-contrast injection for pre-contrast-, late arterial, portal venous-, and delayed-phase images, respectively. The scans were de-identified and downloaded from the picture archiving and communication system (PACS) server. Subsequently, automated image co-registration and whole liver segmentation were performed using a convolutional neural network [17], followed by radiomic feature extraction. Full details on the image processing pipeline can be found in Supplement 1.

Survival model and graded prognostic assessment

A random survival forest (RSF) [18] is a non-parametric method that uses an ensemble of survival trees to analyze right-censored time-to-event data. In this study, we fit an RSF with overall survival (OS) as the dependent variable and the combination of all clinical- and radiomic variables as independent variables (termed "candidate variables"). OS was defined as the period between the imaging date and the date of death of any cause. Patients were censored either at their last date of follow-up, end-of-observation date, or at the date of liver transplantation. The following RSF settings were used: 1000 estimator trees were grown with a minimum of 10 samples to split an internal node, and 15 samples were required at a leaf node with $\sqrt{n}$ variables to consider when looking for the best split. First, all candidate variables with a Pearson correlation coefficient > 0.9 in the development cohort were excluded to reduce multicollinearity. Second, we fit the RSF on the remaining candidate variables and obtained a ranked list of variable importance scores by ten permutations of random shuffling. Third, we re-fit the final survival model on the 30 topmost important variables. To gain further insight and interpretability of the proposed method, we obtained variable importance scores by ten permutations of random shuffling for all included variables. Our method was implemented in Python (v3.8.11) using the scikit-survival package (v0.16.0). Three risk groups were defined from the risk score predictions of the proposed model using the "rhier" function of the R package "rolr" (v1.0), which uses a hierarchical method by applying ordered logrank tests [19], to stratify patients into low-, intermediate-, and high-risk groups. The risk score cutoffs for each risk group were derived from the development cohort, with a minimum of 25 subjects in each risk group. The same cutoff values were then applied for risk group stratification in the independent validation cohort. For performance evaluation of the proposed model and conventional clinical staging scores, we calculated Harrell's C-index [20] and the area under the time-dependent receiver operating characteristic curve (AUC) [21] at 1–5 years after the date of imaging.

Statistical analysis

Statistical analyses were conducted in SPSS (v27), R (v4.1.1), and Python (v3.8.11). p values < .05 were considered statistically significant, and Bonferroni correction was used when comparing multiple groups. Cox proportional hazards regression analysis was used to determine the association of the developed risk score and the proposed risk groups with OS. Median OS (mOS) was calculated, and Kaplan-Meier survival curves were plotted for each risk group and compared using a logrank test. The survival rates of the proposed risk groups were calculated at 1, 3, and 5 years after the date of imaging. To assess the

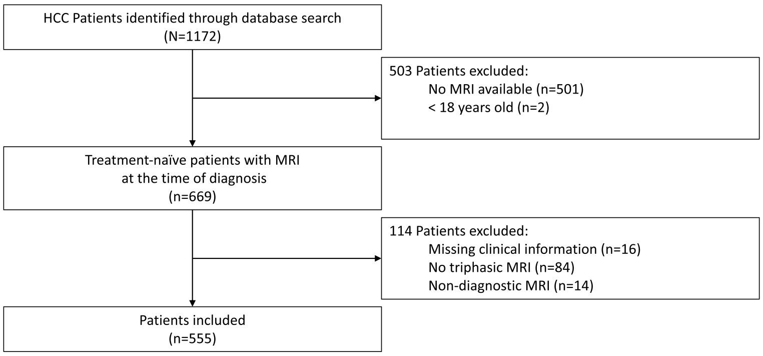

Fig. 1 Flowchart of patient inclusion and exclusion. From an institutional database with 1172 patients, 555 patients (118 females, 437 males, 63.8 ± 8.9 years) with imaging- or histopathologically proven treatment-naïve hepatocellular carcinoma and baseline multiphasic contrast-enhanced magnetic resonance imaging at the time of diagnosis were included in the study

Table 1 Patient baseline characteristics

Characteristic	Overall	Development cohort	Validation cohort	*p* value
Number of patients	555	471	84	
Follow-up (months), median [IQR]	17.43 [25.17]	17.83 [25.28]	15.35 [23.98]	1.00[#]
Dead	287 (51.7)	241 (51.2)	46 (54.8)	1.00[‡]
Demographics				
Age, mean (SD)	63.8 (8.9)	63.9 (9.0)	63.0 (8.5)	1.00[†]
Sex				
Female	118 (21.3)	101 (21.4)	17 (20.2)	1.00[‡]
Male	437 (78.7)	370 (78.6)	67 (79.8)	
Ethnicity*				
Asian	15 (2.7)	15 (3.2)	0 (0.0)	1.00[‡]
Black	72 (13.0)	61 (13.0)	11 (13.1)	
Hispanic	78 (14.1)	69 (14.6)	9 (10.7)	
Other/unknown	6 (1.1)	5 (1.1)	1 (1.2)	
White	384 (69.2)	321 (68.2)	63 (75.0)	
Cirrhosis	526 (94.8)	444 (94.3)	82 (97.6)	1.00[‡]
Etiology				
HCV*	319 (57.5)	271 (57.5)	48 (57.1)	1.00[‡]
HBV*	29 (5.2)	26 (5.5)	3 (3.6)	1.00[‡]
Alcohol	167 (30.1)	136 (28.9)	31 (36.9)	1.00[‡]
NAFLD*	87 (15.7)	77 (16.3)	10 (11.9)	1.00[‡]
Autoimmune	8 (1.4)	8 (1.7)	0 (0.0)	1.00[‡]
Cryptogenic	13 (2.3)	11 (2.3)	2 (2.4)	1.00[‡]
Not available	18 (3.2)	16 (3.4)	2 (2.4)	1.00[‡]
ECOG performance status				
0	405 (73.0)	341 (72.4)	64 (76.2)	1.00[‡]
1	106 (19.1)	94 (20.0)	12 (14.3)	
2	24 (4.3)	21 (4.5)	3 (3.6)	
3	10 (1.8)	7 (1.5)	3 (3.6)	
4	10 (1.8)	8 (1.7)	2 (2.4)	
Radiological data				
Number of lesions, mean (SD)	1.5 (1.1)	1.5 (1.0)	1.8 (1.6)	1.00[†]
Maximum tumor diameter (cm), mean (SD)	4.0 (3.2)	4.0 (3.2)	4.3 (3.4)	1.00[†]
Cumulative tumor diameter (cm), mean (SD)	4.6 (3.7)	4.6 (3.7)	4.9 (3.8)	1.00[†]
Liver lobe				
Bilobar	124 (22.3)	99 (21.0)	25 (29.8)	1.00[‡]
Left	110 (19.8)	95 (20.2)	15 (17.9)	
Right	321 (57.8)	277 (58.8)	44 (52.4)	
Ascites on imaging				
Absent	421 (75.9)	360 (76.4)	61 (72.6)	1.00[‡]
Slight	87 (15.7)	74 (15.7)	13 (15.5)	
Moderate	47 (8.5)	37 (7.9)	10 (11.9)	
Portal vein thrombosis	63 (11.4)	51 (10.8)	12 (14.3)	1.00[‡]
Tumor thrombus	51 (9.2)	41 (8.7)	10 (11.9)	1.00[‡]
Infiltrative disease	28 (5.0)	22 (4.7)	6 (7.1)	1.00[‡]
Metastatic disease	37 (6.7)	27 (5.7)	10 (11.9)	1.00[‡]
Laboratory values				
Alpha-Fetoprotein (ng/mL), mean (SD)	3799.0 (33,226.9)	2864.9 (18,534.2)	9037.1 (73,424.4)	1.00[†]
Total bilirubin (mg/dL), mean (SD)	1.4 (1.8)	1.4 (1.8)	1.5 (2.3)	1.00[†]
Direct bilirubin (mg/dL), mean (SD)	0.7 (1.3)	0.7 (1.3)	0.8 (1.3)	1.00[†]

Table 1 (continued)

Characteristic	Overall	Development cohort	Validation cohort	*p* value
Serum albumin (g/dL), mean (SD)	3.6 (0.6)	3.6 (0.6)	3.5 (0.6)	1.00[†]
Sodium (mmol/L), mean (SD)	137.9 (3.7)	138.0 (3.6)	137.3 (4.1)	1.00[†]
Creatinine (mg/dL), mean (SD)	1.0 (0.4)	1.0 (0.4)	1.0 (0.4)	1.00[†]
International normalized ratio, mean (SD)	1.2 (0.3)	1.2 (0.3)	1.2 (0.3)	1.00[†]
Partial thromboplastin time (sec), mean (SD)	12.7 (5.3)	12.7 (5.6)	12.6 (2.9)	1.00[†]
Staging systems				
Child-Pugh class				
A	336 (60.5)	288 (61.1)	48 (57.1)	1.00[‡]
B	184 (33.2)	156 (33.1)	28 (33.3)	
C	35 (6.3)	27 (5.7)	8 (9.5)	
BCLC* stage				
0	45 (8.1)	40 (8.5)	5 (6.0)	1.00[‡]
A	345 (62.2)	300 (63.7)	45 (53.6)	
B	70 (12.6)	57 (12.1)	13 (15.5)	
C	52 (9.4)	41 (8.7)	11 (13.1)	
D	43 (7.7)	33 (7.0)	10 (11.9)	
First-line treatments				
Transarterial chemoembolization	192 (34.6)	159 (33.8)	33 (39.3)	1.00[‡]
Ablation	138 (24.9)	113 (24.0)	25 (29.8)	
Liver resection	82 (14.8)	75 (15.9)	7 (8.3)	
Combined transarterial chemoembolization + ablation	68 (12.3)	63 (13.4)	5 (6.0)	
Sorafenib	24 (4.3)	19 (4.0)	5 (6.0)	
Best supportive care	24 (4.3)	18 (3.8)	6 (7.1)	
Y90-radioembolization	20 (3.6)	17 (3.6)	3 (3.6)	
Liver transplantation	7 (1.3)	7 (1.5)	0 (0)	

Numbers in parentheses are percentages. Ethnicity is provided through the electronic health record. To assess data consistency, the datasets were compared using a [†]two sample t-test for continuous, a [‡]Chi-squared test for categorical characteristics, and a [#]logrank test for time-to-event data. *HCV*, hepatitis C virus; *HBV*, hepatitis B virus; NAFLD, non-alcoholic fatty liver disease; Child-Pugh [8]; *BCLC*, Barcelona Clinic Liver Cancer [9]

generalizability of the risk groups' survival times to new cohorts, the survival times of each risk group were compared between the development- and validation cohort using a logrank test.

Results

Patient characteristics

A total of 555 patients (mean age, 63.8 years ± 8.9 [standard deviation]; 118 females) with treatment-naïve HCC and multiphasic contrast-enhanced MRI at the time of diagnosis were included in the study. Patients without MRI at baseline ($n = 501$), < 18 years ($n = 2$), missing clinical information ($n = 16$), no triphasic image acquisition ($n = 84$), and non-diagnostic MRI ($n = 14$) were excluded from the study (Fig. 1). Patient baseline characteristics are summarized in Table 1, and MRI parameters are reported in Supplemental Table 1. HCC was either proven by imaging criteria or histopathology.

A total of 287 (51.7%) patients died after a median time of 14.40 months (range, 0.20–97.12 months; interquartile range (IQR), 22.23) after the date of imaging, and patients were followed up for a median of 32.47 months (range: 0.20–118.90 months; IQR: 61.5) after the date of imaging. The median time between the laboratory results and the imaging date was 10 days (IQR, 28.3). First treatments based on the institution's multidisciplinary tumor board decisions were as follows: 192 (34.6%) patients underwent transarterial chemoembolization, 138 (24.9%) thermal ablation, 82 (14.8%) hepatectomy, 68 (12.3%) a combination of transarterial chemoembolization and thermal ablation, 24 (4.3%) Sorafenib, 24 (4.3%) best supportive care, 20 (3.6%) transarterial radioembolization with Yttrium-90, and lastly 7 (1.3%) liver transplantation. For model development and validation, a total of 471 (85%) patients were randomly allocated to the development cohort and 84 (15%) to the independent validation cohort.

Survival model

Figure 2 summarizes the entire model development pipeline. The proposed model attained C-indices of 0.8503 and 0.8234 in the development- and validation cohort, respectively. Table 2 summarizes all performance metrics for the proposed model and conventional clinical staging systems. For the interpretability of the proposed model, Fig. 3 depicts the variable importance scores of the included variables. On average, the proposed framework required a running time of 1.11 min per patient (automated liver segmentation, 0.70 s; extraction of 23 included radiomic features, 1.09 min; model prediction, 0.42 s).

Mortality risk predictions and graded prognostic assessment

The distribution of risk scores in the development and validation cohort is shown in Fig. 4. In the development- and validation cohort, the mean (± standard deviation) predicted risk score was 121.57 (± 65.31) and 135.64 (± 67.59), respectively. Cox proportional hazards regression analysis showed a highly significant association between the predicted risk score and OS in the development cohort (coefficient, 0.021658 (p < .00001); HR, 1.022 (95% CI: 1.02, 1.024)), and in the validation cohort (coefficient, 0.021676 (p <*.00001*); HR, 1.022 (95% CI 1.016, 1.028)). The cutoff values determined by the hierarchical method to stratify patients into low-, intermediate-, and high-risk groups based on the proposed model's predicted risk scores were 93.08 and 172.73. Detailed results of the Cox proportional hazards regression analysis for each risk group can be found in Supplemental Table 2. Example cases are shown in Fig. 5. In the development cohort, 193 (41%) patients were assigned to the low-risk group, 185 (39%) patients to the intermediate-risk group, and 93 (20%) patients to the high-risk group. In the validation cohort, 27 (32%) patients were allocated to the low-risk group, 32 (38%) patients to the intermediate-risk group, and 25 (30%) patients to the high-risk group. Supplemental Table 3 shows a cross-tabulation analysis of the proposed risk groups across conventional clinical staging systems.

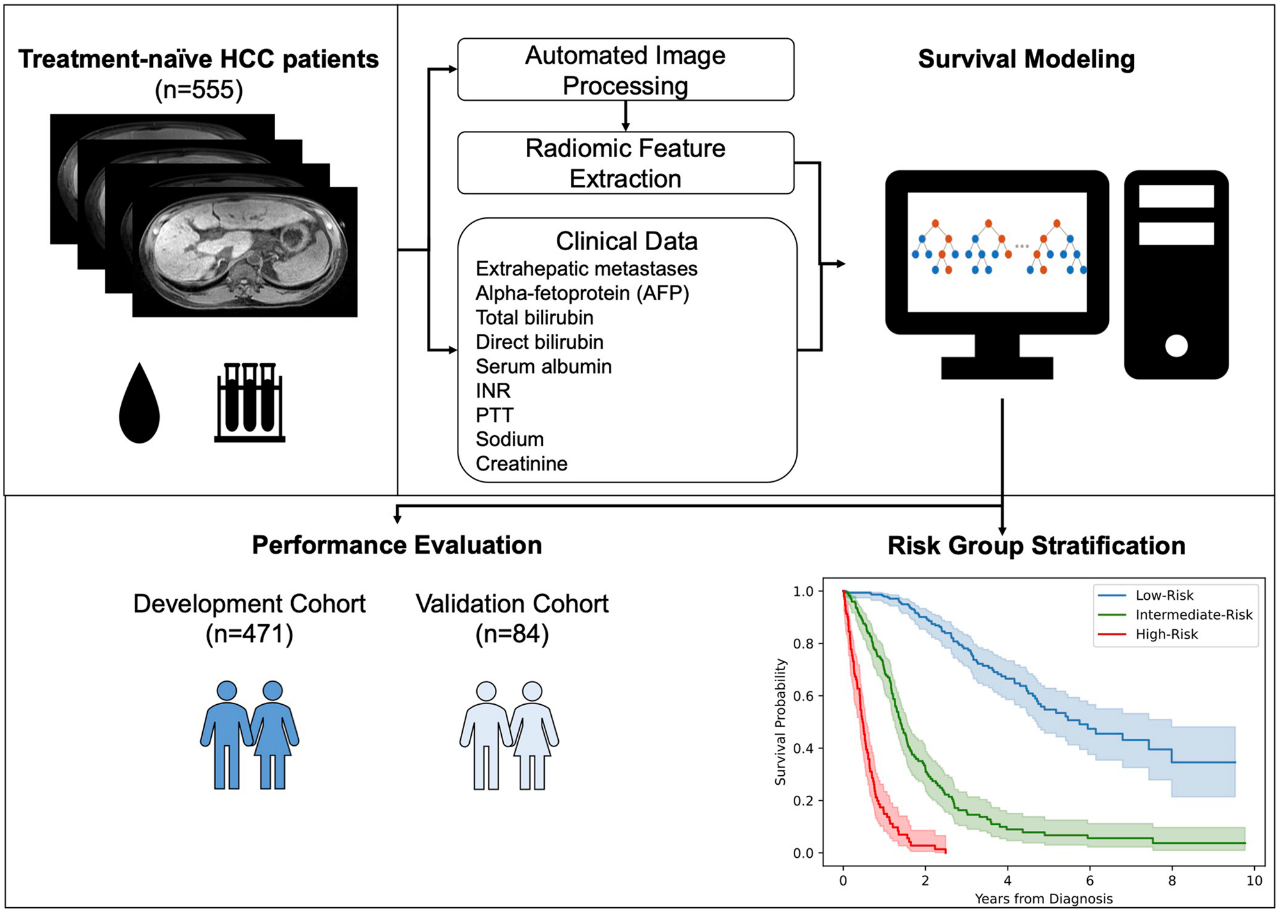

Fig. 2 Model development. An automated liver segmentation framework was adopted for radiomic feature extraction after automated image co-registration. To predict overall survival, a random survival forest was fit from a combination of clinical and radiomic variables. Model performance was evaluated using Harrell's C-index and the area under the time-dependent receiver operating characteristic curve (AUC). Patients were stratified into low-, intermediate-, and high-risk groups based on their predicted risk scores

Survival analysis

A comprehensive table with mOS times and 95% confidence intervals for various strata can be found in Table 3. The mOS time of the entire study cohort was 32.47 (95% CI: 28.40, 37.83) months. In the development- and validation cohort, the mOS were 32.57 (95% CI: 29.13, 38.50) months and 24.57 (95% CI: 14.73, NA) months, respectively. Survival rates (± standard error) for the proposed risk groups in the development- and validation cohort are summarized in Table 4. Survival times between the development- and the validation cohort showed no statistical difference ($p = .29$). In the development cohort, mOS in the low-risk group was 90.40 (95% CI: 62.97, NA) months, 25.8 (95% CI: 23.50, 31.90) months in the intermediate-risk, and 6.40 (95% CI: 5.03, 7.73) months in the high-risk group. In the validation cohort, mOS in the low-risk group was NA (95% CI:48.03, NA) months, 19.60 (95% CI: 14.23, NA) months in the intermediate-risk, and 5.40 (95% CI: 3.80, 12.63) months in the high-risk group. Kaplan-Meier curves for the developed risk groups can be found in Fig. 6. The developed low-, intermediate-, and high-risk groups demonstrated significantly different survival times in both cohorts (development cohort, $p < .0001$; validation cohort, $p < .0001$). Notably, no statistical difference

Table 2 Performance evaluation

	Staging System	Performance Measure					
		C-index	Time-dependent AUC				
			1 year	2 years	3 years	4 years	5 years
Development Cohort (n=471)	Proposed method	0.850	0.907	0.904	0.910	0.890	0.895
	Child-Pugh	0.735	0.721	0.686	0.641	0.630	0.637
	BCLC	0.733	0.808	0.749	0.747	0.748	0.697
	HKLC	0.741	0.807	0.773	0.745	0.730	0.708
	AJCC-TNM	0.699	0.770	0.717	0.707	0.724	0.665
	LCSGJ-TNM	0.697	0.763	0.714	0.712	0.720	0.668
	JIS	0.743	0.818	0.771	0.745	0.747	0.706
	ALBI-Grade	0.589	0.633	0.631	0.611	0.588	0.555
Validation Cohort (n=84)	Proposed method	0.823	0.893	0.867	0.860	0.790	0.765
	Child-Pugh	0.695	0.775	0.715	0.701	0.736	0.718
	BCLC	0.815	0.917	0.850	0.791	0.769	0.799
	HKLC	0.820	0.929	0.822	0.791	0.780	0.797
	AJCC-TNM	0.737	0.825	0.766	0.690	0.700	0.706
	LCSGJ-TNM	0.723	0.813	0.777	0.711	0.635	0.617
	JIS	0.813	0.922	0.855	0.796	0.756	0.734
	ALBI-Grade	0.625	0.635	0.693	0.706	0.701	0.679

To evaluate the performance of mortality risk stratification, we calculated Harrel's C-index [19] and the area under the time-dependent receiver operating characteristic curve [20] ("AUC"). Child-Pugh [8]; *BCLC*, Barcelona Clinic Liver Cancer [9]; *HKLC*, Hong Kong Liver Cancer [10]; *AJCC*, American Joint Committee on Cancer 8th edition [11]; *LCSGJ-TNM*, Liver Cancer Study Group of Japan Tumor Node Metastasis [12]; *JIS*, Japan Integrated Staging [13]; *ALBI*, albumin-bilirubin [14]

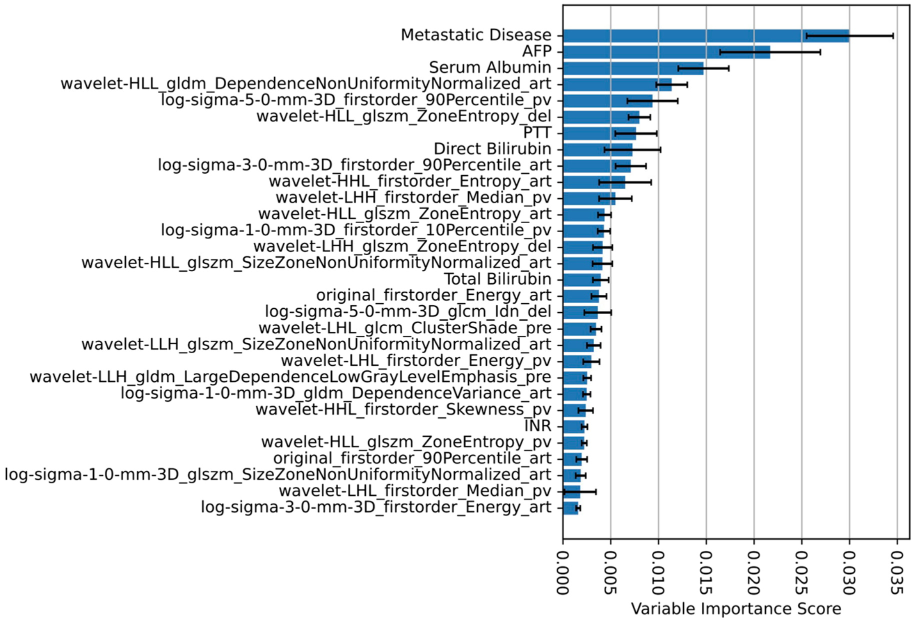

Fig. 3 Variable importance scores. The bar chart shows the mean variable importance score (error bars show standard deviation) of each included variable of the final risk prediction model obtained by 10 permutations of random shuffling. Naming convention of radiomic features: The prefix specifies the image type (original image or filter-derived MR image ("log": Laplacian of Gaussian) with extraction parameters); the suffix specifies the MR contrast phase ("_pre": pre-contrast phase, "_art": late arterial phase, "_pv": portal venous phase, "_del": delayed phase). Equations for the calculation of each radiomic feature are available in ref. [22]. (AFP: Alpha-fetoprotein; INR: international normalized ratio; PTT: partial thromboplastin time)

was found when comparing the survival times of each risk group between the development- and the validation cohort (low-risk group, p = 1.0; intermediate-risk group, p = 1.0; high-risk group, p = 1.0), thus indicating the generalizability of the risk groups' survival times to new data. Complete results of the logrank test for pairwise OS comparisons between the proposed risk groups can be found in Supplemental Table 4. Kaplan-Meier curves for the conventional staging scores can be found in Supplemental Figure 1.

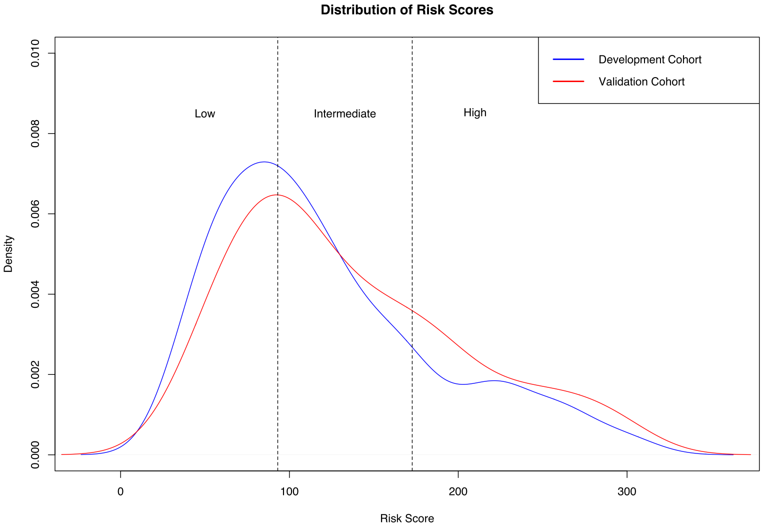

Fig. 4 Distribution of predicted risk scores in the development- and independent validation cohort. Based on the risk score predictions of the survival model in the development cohort, we derived two cutoff points (93.08 and 172.73) to stratify patients into low-, intermediate-, and high-risk groups. We applied the same cutoff points for stratification in the independent validation cohort. For plotting, a Gaussian smoothing kernel was used

Table 3 Median overall survival times across staging systems

Strata	Median OS in months (95% CI)	
	Development cohort	Validation cohort
Entire cohort	32.57 (29.13, 38.5)	24.57 (14.73, NA)
Proposed risk groups		
Low risk	90.4 (62.97, NA)	NA (48.03, NA)
Intermediate risk	25.8 (23.5, 31.9)	19.6 (14.23, NA)
High Risk	6.4 (5, 7.8)	5.4 (3.8, NA)
Child-Pugh		
A	43.6 (36.97, 56.77)	97.17 (24.57, NA)
B	18.6 (15.9, 26.13)	15.37 (6.8, NA)
C	4.83 (2.1, 5.9)	3.92 (1.23, NA)
BCLC stage		
0	74.7 (57.67, NA)	NA (NA, NA)
A	39.8 (32.93, 53.1)	65.77 (36.73, NA)
B	18.33 (16.43, 25.8)	13.67 (9.3, NA)
C	7.73 (5.83, 10.43)	5.4 (4.1, NA)
D	3.5 (2.1, 5.1)	2.65 (1.23, NA)
HKLC stage		
I	57.67 (52.3, 91.6)	NA (36.73, NA)
II	28.63 (24.33, 33.87)	46.3 (23.9, NA)
III	16.93 (15.23, 21.47)	8 (6.5, NA)
IV	9.07 (6.4, NA)	5.47 (4.77, NA)
V	3.27 (2.5, 5.1)	2.65 (1.23, NA)
AJCC-TNM		
IA	57.67 (50.7, 74.7)	65.77 (24.57, NA)
IB	38.5 (30.3, 54.1)	46.3 (14.73, NA)
II	25.23 (21, 35.17)	9.3 (6.5, NA)
IIIA	17.8 (15.83, 44.53)	3.8 (1.6, NA)
IIIB	5.83 (3.7, 16.93)	1.13 (0.23, NA)
IVA	7.97 (1.6, NA)	5.47 (4.77, NA)
IVB	2.67 (2.1, 7.1)	48.03 (20.33, NA)
LCSGJ-TNM		
I	57.67 (50.7, 74.7)	48.03 (36.73, NA)
II	39.8 (32.57, 54.3)	9.83 (8.33, NA)
III	21 (17.4, 29.13)	2.03 (0.23, NA)
IVA	6.78 (3.7, 19.73)	5.47 (4.77, NA)
IVB	2.67 (2.1, 7.1)	NA (27.9, NA)
JIS		
0	59.6 (54.7, NA)	NA (NA, NA)
1	45.7 (32.93, 62.97)	48.03 (27.9, NA)
2	30.3 (21, 42.57)	20.33 (14.73, NA)
3	14.67 (8.53, 19.5)	9.2 (2.03, NA)
4	3.5 (2.23, 7.1)	4.07 (3.8, NA)
5	1.6 (0.5, NA)	0.73 (0.23, NA)
ALBI grade		
1	39.43 (33.87, 53.1)	2.5 (NA, NA)
2	12.13 (3.27, NA)	14.73 (5.7, NA)
3	22.1 (16.67, 27.43)	NA (NA, NA)

NA values indicate that more than 50% of the population was still alive at the end of the analysis; thus, median OS times cannot be calculated. *Child-Pugh* [8]; *BCLC*, Barcelona Clinic Liver Cancer [9]; *HKLC*, Hong Kong Liver Cancer [10]; *AJCC*, American Joint Committee on Cancer 8th edition [11]; *LCSGJ-TNM*, Liver Cancer Study Group of Japan Tumor Node Metastasis [12]; *JIS*, Japan Integrated Staging [13]; *ALBI*, albumin-bilirubin [14]

Discussion

Using a large dataset ($n = 555$), we devised and independently validated a fully automated framework for mortality risk prediction in hepatocellular carcinoma patients using routinely available standard-of-care clinical data and radiomic biomarkers from automated liver segmentations on baseline multiphasic contrast-enhanced MRI. This completely data-driven method yielded reliable, fast, and reproducible risk predictions and attained state-of-the-art performances for mortality risk quantification at baseline. The generalizability of our method was confirmed in an independent validation cohort, and performance was compared against conventional staging systems. In addition, the proposed stratification into low-, intermediate- and high-risk groups yielded similar overall survival times in the development and validation cohort, indicating the generalizability of the method. By using automated liver segmentations, we ensure that the extracted radiomic imaging markers are stable and reproducible and increase the workflow substantially by demonstrating segmentation computation times under a second without the need for human interaction [17]. Finally, we developed our method using a data-driven approach. Instead of stratifying patients into risk groups based on one-dimensional image measurements [9–13], we derived risk group cutoff values using the full three-dimensional imaging volume itself. Thus, such a risk prediction framework could enable personalized follow-up strategies, guide management decisions, and improve clinical workflow efficiency in tumor boards.

We hypothesize that the proposed framework outperformed conventional systems for mortality risk quantification in terms of C-index and AUC as it uses advanced quantitative imaging biomarkers from the whole liver volume in imaging and a data-driven approach for mortality risk prediction. Three-dimensional quantitative assessment of tumor burden has been shown to be a stronger predictor of patient survival than one-dimensional tumor size measurements [23], and one-dimensional tumor size measurements, as used in conventional staging systems, have shown major limitations in reflecting viability, actual tumor size, and growth potential [24]. Our approach uses the full 3D MR imaging data for the extraction of quantitative biomarkers, which is a rich representation of MRI compared to single-dimensional representations such as diameter-based measurements. The 30 biomarkers with the highest importance scores derived from the data demonstrate a combination of clinical features and radiomics across all four phases of the MRI study (Fig. 4). These biomarkers effectively represent disease through intensity patterns and textures summarized by the

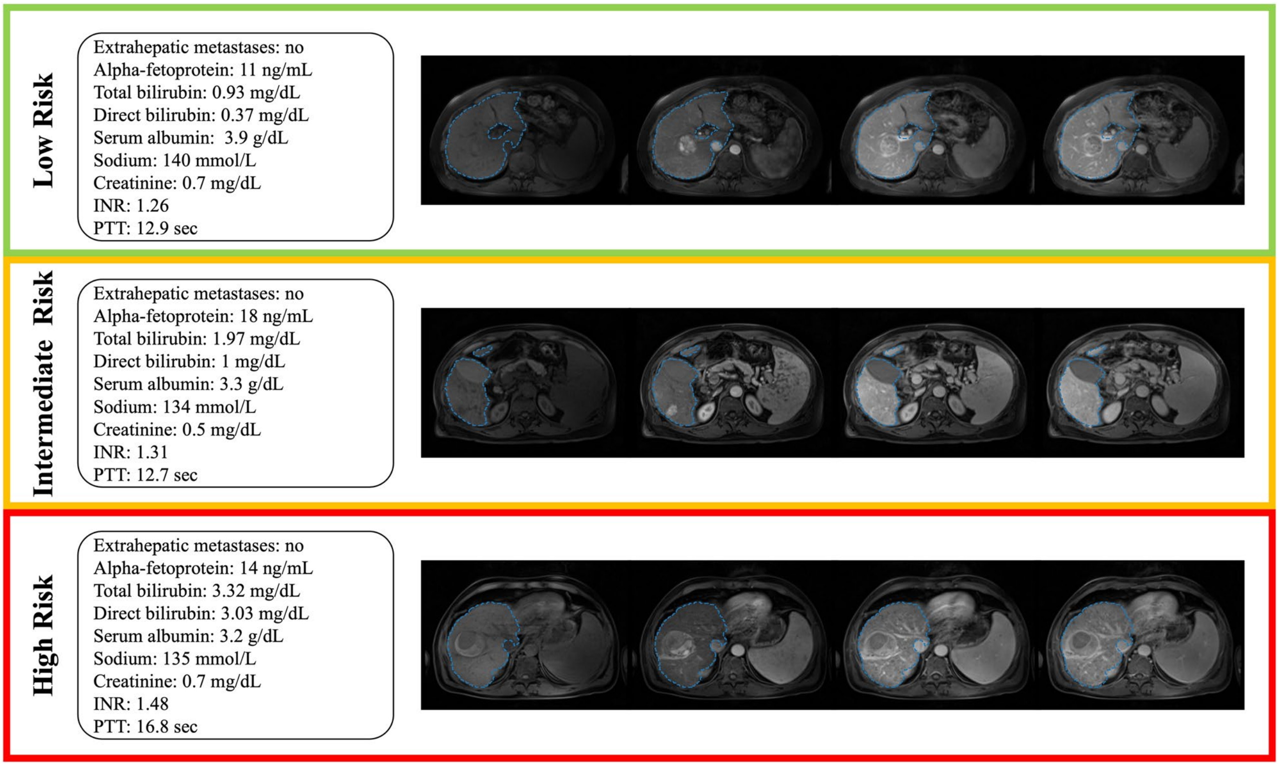

Low Risk:
Extrahepatic metastases: no
Alpha-fetoprotein: 11 ng/mL
Total bilirubin: 0.93 mg/dL
Direct bilirubin: 0.37 mg/dL
Serum albumin: 3.9 g/dL
Sodium: 140 mmol/L
Creatinine: 0.7 mg/dL
INR: 1.26
PTT: 12.9 sec

Intermediate Risk:
Extrahepatic metastases: no
Alpha-fetoprotein: 18 ng/mL
Total bilirubin: 1.97 mg/dL
Direct bilirubin: 1 mg/dL
Serum albumin: 3.3 g/dL
Sodium: 134 mmol/L
Creatinine: 0.5 mg/dL
INR: 1.31
PTT: 12.7 sec

High Risk:
Extrahepatic metastases: no
Alpha-fetoprotein: 14 ng/mL
Total bilirubin: 3.32 mg/dL
Direct bilirubin: 3.03 mg/dL
Serum albumin: 3.2 g/dL
Sodium: 135 mmol/L
Creatinine: 0.7 mg/dL
INR: 1.48
PTT: 16.8 sec

Fig. 5 Example cases. Standard-of-care clinical data and axial pre-contrast-, late arterial, portal venous-, and delayed-phase MRI with corresponding automated liver segmentations overlaid in blue. Low-risk group: A 59-year-old male patient presenting with a focal 4.5 cm lesion in the right liver lobe. The patient was censored after 8.75 years. Intermediate-risk group: A 54-year-old male patient presenting with a focal 3.1 cm lesion in the right liver lobe. The patient died 15 months after diagnosis. High-risk group: A 54-year-old male patient presenting with a focal 5.7 cm lesion in the right liver lobe. The patient died 6.7 months after diagnosis

radiomics in different phases of the imaging study. The performances of the conventional staging systems are in line with previously published studies [25–31]. Previous works have developed machine learning models for mortality risk quantification. However, direct comparison is challenging due to the different datasets, imaging modalities, and study endpoints being used. Mei et al. [32] developed and validated a prognostic nomogram to predict survival in patients with unresectable HCC after hepatic arterial infusion chemotherapy in a cohort with 463 predominantly advanced-stage patients attaining C-indices of 0.710 and 0.716 in their development and validation cohorts, respectively. Furthermore, the authors proposed a risk stratification approach to classify patients into three or four risk groups based on a trisection cutoff and a quartile cutoff point with significantly different OS times. While their approach did not include quantitative imagining biomarkers, their data-driven design achieved superior performance compared to conventional staging systems in their cohort, similar to the findings of our study. Liu et al. [33] developed and validated a prognostic nomogram to predict overall survival in HCC patients after hepatectomy from radiomic features from tumor segmentations on portal venous phase computed tomography and clinical- and pathological variables in a cohort with 544 Chinese patients and achieved C-indices of 0.747 and 0.777 in their development and validation cohorts, respectively. Based on the predicted risk scores, patients were allocated into

Table 4 Survival rates (± standard error) for the proposed risk groups

Proposed risk group	Years	Survival rates (± Standard error)	
		Development cohort (*n* = 471)	Validation cohort (*n* = 84)
Low risk	1	0.98 (± 0.01)	1.00 (± 0.00)
	3	0.85 (± 0.03)	0.85 (± 0.08)
	5	0.61 (± 0.05)	0.68 (± 0.13)
Intermediate risk	1	0.83 (± 0.03)	0.70 (± 0.08)
	3	0.31 (± 0.04)	0.38 (± 0.10)
	5	0.13 (± 0.04)	0.29 (± 0.11)
High risk	1	0.23 (± 0.05)	0.28 (± 0.09)
	3	0.00 (± 0.00)	0.11 (± 0.08)
	5	0.00 (± 0.00)	0.11 (± 0.08)

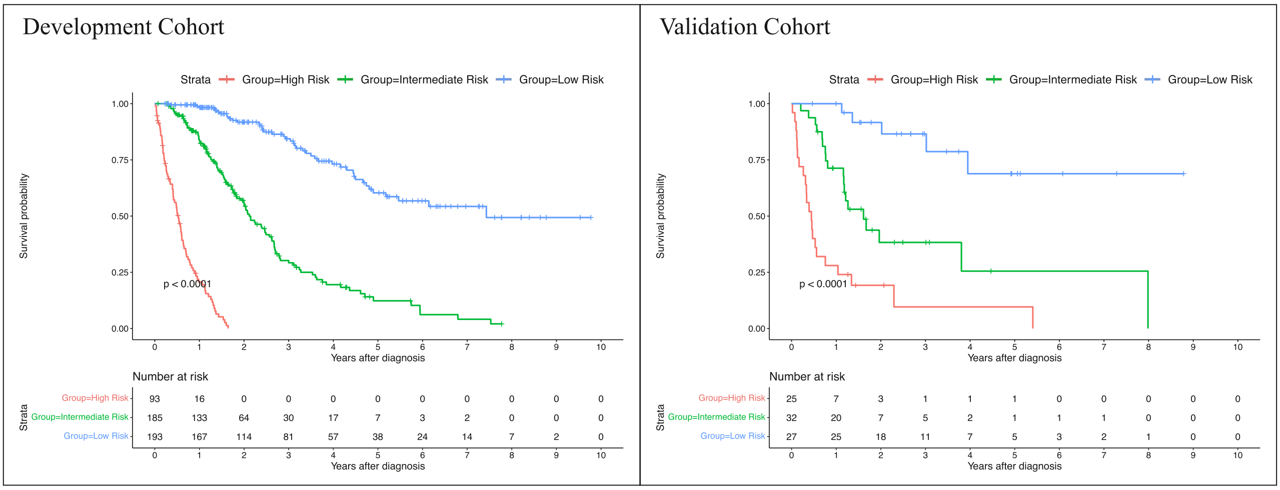

Fig. 6 Kaplan-Meier curves of the proposed risk groups in the development- and validation cohort

low and high-risk groups with significantly different OS times. The authors could significantly improve performance when integrating radiomic features into the risk prediction model compared to clinical- and pathological features alone. Blanc-Durand et al. [34] proposed a scoring system to stratify HCC patients undergoing transarterial radioembolization with Yttrium-90 into a low- and a high-risk group. Radiomic features were derived from semi-automatic liver segmentations from pretreatment ^{18}F-fluorodeoxyglucose positron emission tomography images. Their proposed risk score was significantly correlated with OS and could stratify patients into two risk groups with distinct OS times. However, their method was not evaluated on an independent validation cohort, and no measures of prognostic power, such as the C-index or time-dependent AUCs, were reported, and their method relies on manually revised semi-automatic liver segmentations. In their multi-institutional study, Ji et al. [35] presented a machine learning framework to predict the time to recurrence after resection. Their method was developed and evaluated in 470 patients with solitary HCC lesions and used radiomic features derived from manual tumor and peritumoral segmentations from baseline contrast-enhanced computed tomography images combined with clinical variables and achieved C-indices of 0.733–0.801, outperforming conventional staging systems. The authors proposed a risk stratification approach to allocate patients into low, intermediate, and high-risk groups with significantly different OS times. Their study confirms the utility of a data-driven approach and the usage of advanced quantitative imaging biomarkers for time-to-event data. However, their method relies on time-consuming manual tumor segmentation and does not use a fully automated segmentation method as our liver segmentation approach, which yields segmentation in processing times of under a second (0.70 s).

Our study has several limitations. First, our method was developed using retrospective data from a single institution; thus, prospective multicenter studies and external validation are warranted before potential clinical translation. However, our method was developed using a large dataset and yielded precise and generalizable results in an independent validation cohort. Furthermore, the large cohort size of this study adds a degree of robustness to the findings, and the relative simplicity of the analytical elements involved enhances the likelihood of reproducibility and the reliability of the findings. Due to these factors, we anticipate that other groups can replicate our study using the publicly available code. Second, we did not control for the effects of different treatment types on OS. Nevertheless, our method is still predictive of OS even without any treatment information given. Finally, the proposed method relies on multiphasic contrast-enhanced MRI and cannot be applied to patients who underwent other imaging modalities at baseline. In future work, we will incorporate longitudinal data from multiple external contributors and evaluate our method on a larger independent validation cohort.

In conclusion, we present a fully automated framework for mortality risk prediction in hepatocellular carcinoma patients using routinely available standard-of-care clinical data and radiomic features derived from automated liver segmentations on baseline multiphasic contrast-enhanced MRI outperforming conventional staging systems for mortality risk quantification. The developed method, based on machine learning, can help personalize follow-up strategies, guide management decisions, and improve clinical workflow efficiency in tumor boards.

Abbreviations

AFP	Alpha-fetoprotein
AUC	Area under the curve
CI	Confidence interval
CT	Computed tomography
HCC	Hepatocellular carcinoma
INR	International normalized ratio
IQR	Interquartile range
mOS	Median overall survival
MRI	Magnetic resonance imaging
NA	Not available
PTT	Partial thromboplastin time
RSF	Random survival forest
SD	Standard deviation

Supplementary Information

The online version contains supplementary material available at https://doi.org/10.1007/s00330-024-10624-8.

Below is the link to the electronic supplementary material.Supplementary file1 (DOCX 24.4 MB)

Funding

Open Access funding enabled and organized by Projekt DEAL. J.A.O. was supported by the National Institute of Diabetes and Digestive and Kidney Diseases of the National Institutes of Health under Award Number P30 KD034989 and M.S. the National Institutes of Health Grant Award Number DDRCC DK034989-36 for the Clinical Translational Core of the Yale Liver Center. The content is solely the responsibility of the authors and does not necessarily represent the official views of the Nation Institutes of Health. M.G. was supported by a travel stipend from the Rolf W. Günther Foundation for Radiological Sciences for travel to Yale University. The funders had no role in study design, data collection and analysis, decision to publish, or preparation of the manuscript.

Declarations

Guarantor

The scientific guarantor of this publication is Dr. John Onofrey.

Conflict of interest

The authors of this manuscript declare no relationships with any companies whose products or services may be related to the subject matter of the article.

Statistics and biometry

No complex statistical methods were necessary for this paper.

Informed consent

Written informed consent was waived by the Institutional Review Board.

Ethical approval

This study was approved by the Yale School of Medicine institutional review board with full waiver of consent and conducted in accordance with the declaration of Helsinki.

Study subjects or cohorts overlap

None.

Methodology

- retrospective
- experimental
- performed at one institution

Author details

[1]Department of Radiology and Biomedical Imaging, Yale University School of Medicine, New Haven, CT, USA. [2]Charité Center for Diagnostic and Interventional Radiology, Charité - Universitätsmedizin Berlin, Berlin, Germany. [3]Department of Otorhinolaryngology, University Hospital of Ludwig Maximilians Universität München, Munich, Germany. [4]Department of Biomedical Engineering, Yale University, New Haven, CT, USA. [5]Department of Diagnostic and Interventional Radiology, Pediatric Radiology and Neuroradiology, Rostock University Medical Center, Rostock, Germany. [6]Department of Internal Medicine, Yale University School of Medicine, New Haven, CT, USA. [7]Department of Urology, Yale University School of Medicine, New Haven, CT, USA.

Received: 31 August 2023 Revised: 18 December 2023 Accepted: 8 January 2024
Published online: 27 March 2024

References

1. Sung H, Ferlay J, Siegel RL et al (2021) Global Cancer Statistics 2020: GLOBOCAN estimates of incidence and mortality worldwide for 36 cancers in 185 countries. CA Cancer J Clin 71:209–249
2. Jemal A, Bray F, Center MM, Ferlay J, Ward E, Forman D (2011) Global cancer statistics. CA Cancer J Clin 61:69–90
3. Siegel RL, Miller KD, Jemal A (2019) Cancer statistics, 2019. CA Cancer J Clin 69:7–34
4. White DL, Thrift AP, Kanwal F, Davila J, El-Serag HB (2017) Incidence of hepatocellular carcinoma in All 50 United States, From 2000 Through 2012. Gastroenterology 152:812-820.e815
5. Perz JF, Armstrong GL, Farrington LA, Hutin YJ, Bell BP (2006) The contributions of hepatitis B virus and hepatitis C virus infections to cirrhosis and primary liver cancer worldwide. J Hepatol 45:529–538
6. Chernyak V, Fowler KJ, Kamaya A et al (2018) Liver Imaging Reporting and Data System (LI-RADS) version 2018: imaging of hepatocellular carcinoma in at-risk patients. Radiology 289:816–830
7. Hamer OW, Schlottmann K, Sirlin CB, Feuerbach S (2007) Technology insight: advances in liver imaging. Nat Clin Pract Gastroenterol Hepatol 4:215–228
8. Child CG, Turcotte JG (1964) Surgery and portal hypertension. Major Probl Clin Surg 1:1–85
9. Reig M, Forner A, Rimola J et al (2022) BCLC strategy for prognosis prediction and treatment recommendation: the 2022 update. J Hepatol 76:681–693
10. Yau T, Tang VY, Yao TJ, Fan ST, Lo CM, Poon RT (2014) Development of Hong Kong Liver Cancer staging system with treatment stratification for patients with hepatocellular carcinoma. Gastroenterology 146:1691–1700
11. Amin MB, Greene FL, Edge SB et al (2017) The Eighth Edition AJCC Cancer Staging Manual: Continuing to build a bridge from a population-based to a more "personalized" approach to cancer staging. CA Cancer J Clin 67:93–99
12. Japan TLCSGo (1989) The general rules for the clinical and pathological study of primary liver cancer. Jpn J Surg 19:98–129
13. Kudo M, Chung H, Osaki Y (2003) Prognostic staging system for hepatocellular carcinoma (CLIP score): its value and limitations, and a proposal for a new staging system, the Japan Integrated Staging Score (JIS score). J Gastroenterol 38:207–215
14. Johnson PJ, Berhane S, Kagebayashi C et al (2015) Assessment of liver function in patients with hepatocellular carcinoma: a new evidence-based approach-the ALBI grade. J Clin Oncol 33:550–558
15. Tacher V, Lin M, Duran R et al (2016) Comparison of existing response criteria in patients with hepatocellular carcinoma treated with transarterial chemoembolization using a 3D quantitative approach. Radiology 278:275–284
16. Gross M, Spektor M, Jaffe A et al (2021) Improved performance and consistency of deep learning 3D liver segmentation with heterogeneous cancer stages in magnetic resonance imaging. PLoS One 16:e0260630
17. Gross M, Huber S, Arora S et al (2024) Automated MRI liver segmentation for anatomical segmentation, liver volumetry, and the extraction of radiomics. Eur Radiol. https://doi.org/10.1007/s00330-023-10495-5

18. Ishwaran H, Kogalur UB, Blackstone EH, Lauer MS (2008) Random survival forests. Ann Appl Statist 2:841–860
19. Crowley J, Mitchell A, Qu P, Morgan G, Barlogie B (2017) Optimal three group splits based on a survival outcome. Frontiers of Biostatistical Methods and Applications in Clinical Oncology:231–242. https://doi.org/10.1007/978-981-10-0126-0_14
20. Harrell FE Jr, Lee KL, Mark DB (1996) Multivariable prognostic models: issues in developing models, evaluating assumptions and adequacy, and measuring and reducing errors. Stat Med 15:361–387
21. Blanche P, Dartigues JF, Jacqmin-Gadda H (2013) Estimating and comparing time-dependent areas under receiver operating characteristic curves for censored event times with competing risks. Stat Med 32:5381–5397
22. Pyradiomics-community (February 11, 2020) pyradiomics Documentation Release v3.0. Available via https://pyradiomics.readthedocs.io/en/v3.0/features.html. Accessed 2023 Feb 24
23. Park T, Yoon MA, Cho YC et al (2022) Automated segmentation of the fractured vertebrae on CT and its applicability in a radiomics model to predict fracture malignancy. Sci Rep 12:6735
24. Zhao Y, Zhao T, Chen S et al (2022) Fully automated radiomic screening pipeline for osteoporosis and abnormal bone density with a deep learning-based segmentation using a short lumbar mDixon sequence. Quant Imaging Med Surg 12:1198–1213
25. Kim KM, Sinn DH, Jung SH et al (2016) The recommended treatment algorithms of the BCLC and HKLC staging systems: does following these always improve survival rates for HCC patients? Liver Int 36:1490–1497
26. Adhoute X, Penaranda G, Raoul JL, Bourliere M (2017) Usefulness of the MESH score in a European hepatocellular carcinoma cohort. World J Hepatol 9:711–714
27. Zhao S, Wang M, Yang Z et al (2020) Comparison between Child-Pugh score and Albumin-Bilirubin grade in the prognosis of patients with HCC after liver resection using time-dependent ROC. Ann Transl Med 8:539
28. op den Winkel M, Nagel D, Sappl J et al (2012) Prognosis of patients with hepatocellular carcinoma Validation and ranking of established staging-systems in a large western HCC-cohort. PLoS One 7:e45066
29. Gui B, Weiner AA, Nosher J et al (2018) Assessment of the albumin-bilirubin (ALBI) grade as a prognostic indicator for hepatocellular carcinoma patients treated with radioembolization. Am J Clin Oncol 41:861–866
30. Bai Y, Lian Y, Wu J et al (2021) A prognostic scoring system for predicting overall survival of patients with the TNM 8th edition stage I and II hepatocellular carcinoma after surgery: a population-based study. Cancer Manag Res 13:2131–2142
31. Parikh ND, Scaglione S, Li Y et al (2018) A comparison of staging systems for hepatocellular carcinoma in a multicenter US cohort. Clin Gastroenterol Hepatol 16:781–782
32. Mei J, Lin WP, Shi F et al (2021) Prognostic nomogram predicting survival of patients with unresectable hepatocellular carcinoma after hepatic arterial infusion chemotherapy. Eur J Radiol 142:109890
33. Liu Q, Li J, Liu F et al (2020) A radiomics nomogram for the prediction of overall survival in patients with hepatocellular carcinoma after hepatectomy. Cancer Imaging 20:82
34. Blanc-Durand P, Van Der Gucht A, Jreige M et al (2018) Signature of survival: a (18)F-FDG PET based whole-liver radiomic analysis predicts survival after (90)Y-TARE for hepatocellular carcinoma. Oncotarget 9:4549–4558
35. Ji GW, Zhu FP, Xu Q et al (2019) Machine-learning analysis of contrast-enhanced CT radiomics predicts recurrence of hepatocellular carcinoma after resection: a multi-institutional study. EBioMedicine 50:156–165

Publisher's Note

Springer Nature remains neutral with regard to jurisdictional claims in published maps and institutional affiliations.